RSC Advances

PAPER

Cite this: *RSC Adv.*, 2020, **10**, 36627

In situ synthesis of copper nanoparticles encapsulated by nitrogen-doped graphene at room temperature *via* solution plasma†

Phu Quoc Phan, [a] Sangwoo Chae, [ac] Phuwadej Pornaroontham, [ac] Yukihiro Muta, [ac] Kyusung Kim, [e] Xiaoyang Wang [ad] and Nagahiro Saito *[abcd]

Received 20th August 2020
Accepted 18th September 2020

DOI: 10.1039/d0ra07162e

rsc.li/rsc-advances

Metal–carbon core–shell nanostructures have gained research interest due to their better performances in not only stability but also other properties, such as catalytic, optical, and electrical properties. However, they are limited by complicated synthesis approaches. Therefore, the development of a simple method for the synthesis of metal–carbon core–shell nanostructures is of great significance. In this work, a novel Cu–core encapsulated by a N-doped few-layer graphene shell was successfully synthesized in a one-pot in-liquid plasma discharge, so-called solution plasma (SP), to our knowledge for the first time. The synthesis was conducted at room temperature and atmospheric pressure by using a pair of copper electrodes submerged in a DMF solution as the precursor. The core–shell structure of the obtained products was confirmed by HR-TEM, while further insight information was explained from the results of XRD, Raman, and XPS measurements. The obtained Cu-core encapsulated by the N-doped few-layer graphene shell demonstrated relatively high stability in acid media, compared to the commercial bare Cu particles. Moreover, the stability was found to depend on the thickness of the N-doped few-layer graphene shell which can be tuned by adjusting the SP operating conditions.

1. Introduction

Graphene is a 2D material that has received extensive attention in both research and industrial fields for the last few decades due to its attractive properties.[1] Graphene has a large specific surface area, excellent electrical conductivity, good mechanical flexibility and, especially, strong thermal/chemical stability.[2] Thus, it has shown potential to be used as a protective shell for metal nanoparticles from some hazardous environments, such as acid corrosion and oxidation, which can be beneficial in several applications.[3] The protective ability, when graphene is used as a shell, depends on the number of graphene layers.[3] A graphene bilayer previously was reported that blocked the diffusion of oxygen to the core by posing a high-energy barrier, resulting in the better protection from oxidation.[4] However, in some cases, such as being used as a catalyst in electrochemical oxygen reduction reaction, when the metal nanoparticles are encapsulated in the graphene layers, the surface activeness of the products after encapsulation is lowered. The lowering of the surface activeness leads to hindrance of their electrocatalytic activity.[4] This phenomenon was reported that it was caused by the presence of the only sp^2 hybridized carbon–carbon bonding in the structure of graphene, which was the outer surface of the encapsulated nanoparticles.[4] Accordingly, the modification of the graphene shell is still needed, aiming to enhance the surface activeness. Introduction of heteroatoms into the carbon framework generally can provide the electropositive sites, as active sites, on the carbon material, owing to the different electronegativity between a carbon atom and heteroatoms.[5] Therefore, the encapsulation of metal nanoparticles by heteroatom-doped graphenes, such as nitrogen-doped graphene (NG), does not only improve the chemical stability but also the surface activeness of the obtained products.

The preparation of metal nanoparticles encapsulated in carbon layers can be effectively conducted by several methods, such as thermal treatment and chemical vapor deposition (CVD).[3,6,7] The method that has been widely used in industries is thermal treatment. The thermal treatment is simple and can be operated at approximately 300 °C, but often resulted in

[a]Department of Chemical Systems Engineering, Graduate School of Engineering, Nagoya University, Furo-cho, Chikusa-ku, Nagoya 464-8603, Japan. E-mail: hiro@sp.material.nagoya-u.ac.jp

[b]Conjoint Research Laboratory in Nagoya University, Shinshu University, Furo-cho, Chikusa-ku, Nagoya 464-8603, Japan

[c]Japan Science and Technology Corporation (JST), Open Innovation Platform with Enterprises, Research Institute and Academia (OPERA), Furo-cho, Chikusa-ku, Nagoya 464-8603, Japan

[d]Japan Science and Technology Corporation (JST), Strategic International Collaborative Research Program (SICORP), Furo-cho, Chikusa-ku, Nagoya 464-8603, Japan

[e]National Institute of Advanced Industrial Science and Technology (AIST), Anagahora, Shimoshidami, Moriyama, Nagoya 463-8560, Japan

† Electronic supplementary information (ESI) available. See DOI: 10.1039/d0ra07162e

amorphous carbon with relatively low conductivity.[8] On the other hand, CVD has shown as one of the promising methods that can produce the high-quality graphene and introduce to the surface of metals.[6,9] However, a large amount of inert gas consumption and relatively high temperature (>700 °C) are required, leading to the high-cost production of the graphene-encapsulated metal nanoparticles. Moreover, by using CVD, the encapsulation of some metal nanoparticles, such as copper (Cu) nanoparticles, was reported to be difficult. The formation of the graphene layer on the surface of Cu nanoparticles was found to be single-layer graphene, rather than multi-layer graphene.[3,10] The formed single-layer graphene can passivate the Cu surface and hinder the further formation of graphene layers. Besides, the growth temperature of graphene, in some cases, was reported to be relatively high (1000 °C), which is almost the same as the melting point of Cu (1085 °C).[11] Therefore, the synthesis of the metal nanoparticles, such as Cu nanoparticles, encapsulated by graphene with the optimal number of layers is still challenging.

Recently, a newly developed electrical discharge process, so-called solution plasma (SP), has been reported that it can simply synthesize metal nanoparticles and heteroatom doped carbon material under ambient conditions, *i.e.*, relatively low temperature and atmospheric pressure.[12,13] In the SP system, a non-equilibrium plasma is generated at tips of metal-rod-type electrodes, immerged under a liquid phase (*e.g.*, an aqueous solution or an organic compound),[14] as shown in Fig. 1. The generated plasma zone has a high temperature (~3700 °C) enough for the formation of graphene, while the surrounding solution can help to reduce the reaction temperature to suit the formation of metal nanoparticles.[14,15] Moreover, various combinations of solutions, electrode materials, and power supply conditions can lead to a variety of reactions and products.[14] Hence, the NG was reported that it could be successfully produced *via* the decomposition and recombination of the organic solvent containing nitrogen in the SP process.[16] Besides, the synthesis of metal nanoparticles can be conducted by using different types of metal electrodes.[17] In the SP process, the rapid bombardment of energetic ions at the tip of these metal electrodes was reported to lead to erosion of metal electrode, diffusion of metal ions, and formation of metal clusters.[13] According to these phenomena, the fabrication of metal nanoparticles, such Cu nanoparticles, encapsulated by NG should be rapidly conducted in one-pot reaction *via* the SP process with low chemical utilization.

In this work, the SP process was successfully used to synthesize core–shell nanostructured materials for the first time. A pair of Cu electrodes were submerged under *N*,*N*-dimethylformamide (DMF) solution in the SP reactor to prepare the Cu nanoparticles encapsulated by nitrogen-doped few-layer graphene (Cu-NFG) at different repetition frequency *via* SP process. The reason that DMF was chosen to act as a precursor of NFG is an aliphaticity of DMF. It could synthesize a few layers of graphene which is not like in case of using an aromatic compound, benzene, that would form carbon nanoparticles due to its much faster synthesis rate.[12] In this research, not only the structure characterizations but also the insight information into the core–shell formation mechanism *via* the SP process were conducted. Finally, the protective ability of SP-induced NG against the acid corrosion and oxidation of Cu nanoparticles was also evaluated.

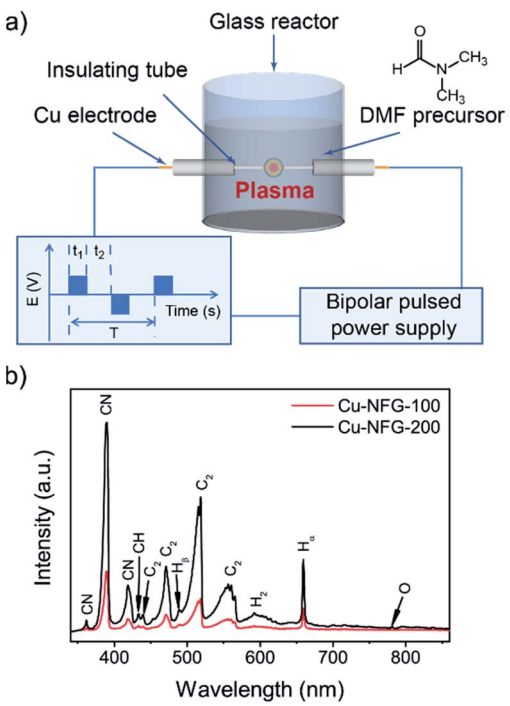

Fig. 1 Schematic of SP process setup (a), and OES spectra during solution plasma for Cu-NFG-100 and Cu-NFG-200 (b).

2. Experimental procedure

2.1 Solution plasma (SP) synthesis

The setup of the SP process was demonstrated in Fig. 1a. A 100 ml of DMF (C_3H_7NO, 99.5% purity, Kanto Chemical Co., Inc., Japan) was poured into a glass reactor connected with a pair of Cu electrodes with a diameter of 4.0 mm (99.9% purity, Nilaco Co., Japan) insulated by ceramic tubes. The gap between electrodes was fixed to be 0.5 mm. The electrodes were connected to a bipolar-pulse power supply (Bipolar-DC pulsed power supply, Kurita Seisakusho Co., Ltd., Japan). The plasma was generated in liquid for 1 h by the fixed supplying voltage and pulse width at 1 kV and 1 μs, respectively. Cu-NFG products were synthesized by varying repetition frequencies (*i.e.*, 100 and 200 kHz). After the SP-induced reaction, the obtained solid residues were filtered through a PTFE filter membrane (JVWP04700, pore size 0.1 μm, Merck) and repeatedly washed with acetone (purity > 99.5%, Kanto Chemical Co., Inc., Japan). The residues were collected and then dried in an oven at 100 °C for 12 h. After that, the samples were collected and weighted to determine the synthesis rate then kept in dark bottles and stored in a desiccator for further characterizations. The Cu-NFG products prepared by different frequencies at 100 and 200 kHz were assigned as Cu-NFG-100 and Cu-NFG-200, respectively.

2.2 Characterizations

Optical emission spectroscopy (OES, UV/Vis USB 2000+, Ocean Optics Inc., USA) was applied for understanding the radical species during the SP process. The core–shell structures and morphologies of the obtained samples were examined by transmission electron microscope (TEM, JEM-2500SE, JEOL Ltd., Japan) at an accelerating voltage of 200 kV. The crystallinity was confirmed and compared with a commercial Cu nanoparticle (25 nm particle size, Sigma-Aldrich, Germany) using X-ray diffraction (XRD, SmartLab, Rigaku Co., Japan) with Cu Kα radiation ($\lambda = 0.154$ nm). Raman spectroscopy (Raman, Leica DM 2500M Ren (RL/TL) microscope, Renishaw Plc., England) was also used to analyze the structure and defects of NFG with a laser-excitation wavelength of 532.5 nm. Mass compositions of the obtained samples were also determined by thermal gravimetric analysis (TGA, TGA&DTG-60AH, Shimadzu Co., Japan) with a heating rate of 10 °C min^{-1} in air and X-ray photoelectron spectroscopy (XPS, PHI 5000 Versa Probe II, ULVAC-PHI, Inc., Japan) using an Mg Kα X-ray source was used to analyze the chemical structure of the obtained samples. The XPS spectra were then deconvoluted using Shirley background subtraction. The resistivities of the synthesized samples were tested by a two-probe method using a Digital Multimeter CDM-2000D. The prepared samples were filled in a 0.3 cm-inner-diameter Teflon cylinder. Then it was compressed using brass pistons. The electrical resistivity was measured with compression at 0.6 MPa. The discharge voltage and current waveforms were measured using a digital oscilloscope (Yokogawa DLM2024-200 MHz Mixed Signal Oscilloscope, Yokogawa Electric Co., Japan). Nitrogen adsorption–desorption measurements were obtained using the adsorption apparatus (BELSORP-mini II, BEL, Japan) at −196 °C for determining the surface area and pore volume distribution results of the obtained samples.

2.3 Immersion test in acid solution

The chemical resistance ability of the obtained Cu-NFG products from acid corrosion and oxidation reaction was investigated by immersion test in acid. To imitate the condition for using in acid, we conducted the immersion test with two different strong acids, 1 N nitric acid (HNO_3, 69.0–70.0% purity, Kanto Chemical Co., Inc., Japan) and 1 N sulfuric acid (H_2SO_4, 0.5 M, Kanto Chemical Co., Inc., Japan) according to ISO 11130 with modification. The immersion in HNO_3 was done under room temperature of 25 °C, while in H_2SO_4 was at 80 °C. All experiments were carried out by immersing 10 mg of each sample into 165 ml of the acid solution. The immersion times were varied to be 1, 2, 4, 8, and 48 h. After reaching to the studied immersion time, the solution was sampled and measured a concentration of metal ion, which was dissolved from the samples by inductively coupled plasma atomic emission spectroscopy (ICP-OES, SPS7800, Hitachi Corp., Japan). Then the mass loss and corrosion rate were calculated using the following equations:

(i) Mass loss:

$$m_{\mathrm{Cu,\ loss}} = \frac{C_{\mathrm{Cu}} \times V_{\mathrm{dd}}}{1000}(g) \quad (1)$$

(ii) Corrosion rate:

$$W = \frac{m_{\mathrm{Cu,\ loss}}}{M \times m_{\mathrm{Cu}} \times A \times t}\left(\mathrm{mol\ cm^{-2}\ h^{-1}}\right) \quad (2)$$

where C_{Cu} is the Cu ion concentration in the collected solution (ppm), V_{dd} is the volume of the tested solution (l), M is the molar mass of Cu (g mol^{-1}), m_{Cu} is the amount of the tested sample (g), A is the surface area of the tested sample (cm^2 g^{-1}), $t$is immersion time (h).

In comparison with commercial products, the purchased commercial Cu powder and Cu particles obtained by cutting from Cu electrode using a diamond file (Diamond thin hand form, # 150, Tsubosan file Co., Ltd., Japan) were also tested with the corresponding procedure.

3. Results and discussion

3.1 Structural characterization

During the plasma discharge in DMF using a pair of Cu electrodes, reddish-gray particles were continuously generated (Fig. S1†). According to the previous report, the SP process could produce nitrogen-doped carbon materials from the nitrogen-containing organic precursors.[18,19] The reddish-gray particles could be suggested to be the combination of nitrogen-doped carbon and Cu nanoparticles which could be occurred through the decomposition and recombination of DMF and the simultaneous sputtering of Cu electrode together.[17,20] OES spectra were obtained to monitor the excited radicals generated in the reaction solutions during the SP process at repetition frequencies of 100 and 200 kHz. Fig. 1b shows that the C_2, CH, CN, H, and O species were generated in both samples, due to the dissociation of DMF molecules.[21,22] An increase in the intensity of emission peaks of the reactive species was observed as increasing the repetition frequency from 100 to 200 kHz. It could imply that higher repetition frequency resulted in higher amounts of radicals in the SP system. These generated reactive species could lead to the continuous collision and dissociation of the surrounded molecules.[23] Moreover, the production rates were also determined and found to be influenced by the repetition frequency. The SP process with higher repetition frequency could give the higher production rates which were found to be 5.2 mg h^{-1} and 15.8 mg h^{-1} for Cu-NFG-100 and Cu-NFG-200, respectively. This could be related to the higher sputtering rate of Cu electrode, when the higher repetition frequency was used, leading to the enhanced formation of Cu nanoparticles.[24]

Furthermore, morphologies of Cu-NFG-100 and Cu-NFG-200 were investigated by low-resolution and high-resolution TEM, as shown in Fig. 2. The presence of black cores and grayish edges were representing a Cu–core and a carbon–shell, respectively. The interplanar lattice space was found to be 0.21 nm, corresponding to that of Cu nanoparticles.[25] The particle size of Cu-NFG-100 was ranging from 5 nm to 11 nm, as shown in the inset of Fig. 2a. The average particle size was calculated to be

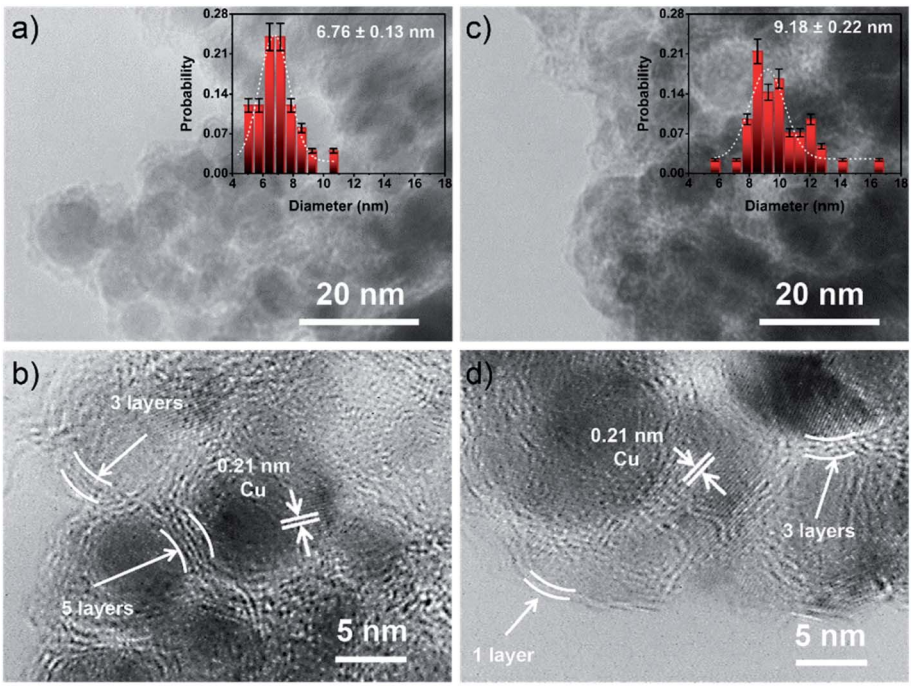

Fig. 2 TEM and HR-TEM images of Cu-NFG-100 (a and b) and Cu-NFG-200 (c and d), respectively.

approximately 6.8 nm. Besides, the high-resolution TEM image in Fig. 2b indicated that the shells contained 3 to 5 layers, which were reported as the suitable number of carbon layers that could promote the synergistic effect to protect the internal core and improve catalytic performance.[3,26] A similar structure was also demonstrated for the Cu-NFG-200, as shown in Fig. 2c and d. The average particle size of 9.2 nm with size distribution ranging from 5 to 17 nm. The obtained result could be caused by the increment of the operating frequency, which could lead to a higher rate of metal sputtering, resulting in not only higher amount but also larger size of Cu nanoparticles.[27] However, fewer layers of carbon shell (*i.e.*, 1 to 3 layers) and some incompletely-covered core were observed, referring to less amount of carbon in Cu-NFG-200, compared to that of Cu-NFG-100. The result was consistent with the TGA result, which revealed that Cu-NFG-100 and Cu-NFG-200 contained carbon content at 18 and 10 wt%, respectively (Fig. S2†). Accordingly, the size of Cu-core and the number of encapsulating layers should be controllable by adjusting the operating frequency in the SP process.

The structural information of the obtained samples was further studied by using XRD. Fig. 3a shows the XRD pattern of the Cu-NFG-100 sample, which presented only characteristic peaks of Cu at 43.18°, 50.32°, and 74.04°, attributing to 111, 200 and 220 planes, respectively.[28] It indicated that the main component in the core structure is Cu metal. On the other hand, the XRD pattern of the Cu-NFG-200 showed not only the characteristic peaks of the Cu metal but also the additional peaks at 35.48°, 38.83°, and 36.49°, which represented to 002 and 111 planes of CuO, and 111 plane of Cu_2O, respectively.[29] The presence of these oxide species could refer to the oxidation of Cu-NFG-200, due to the incomplete encapsulation of the carbon shell. A similar XRD result was also obtained for the oxidized commercial Cu (Fig. S3†). Moreover, the broad peak at 25°, corresponding to 002 plane of carbon, could be observed and it

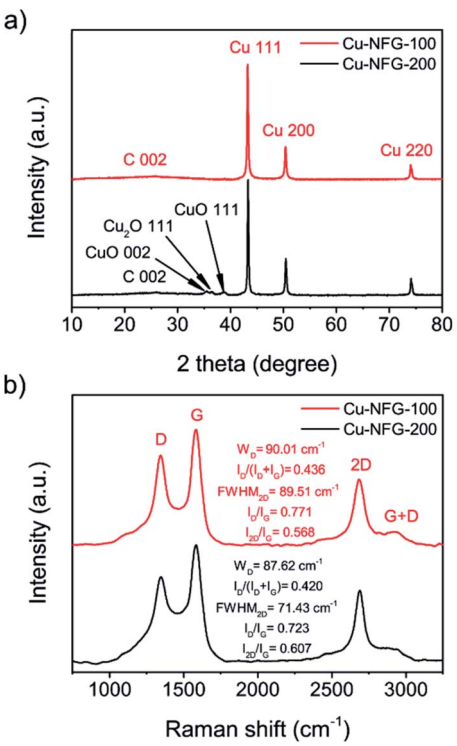

Fig. 3 XRD patterns (a), and Raman spectra (b) of Cu-NFG-100 and Cu-NFG-200.

was previously reported to be the characteristic peak of graphene.[30] Furthermore, Raman measurements were also conducted to investigate the structural information of the graphene shell. The results were shown in Fig. 3b. The Raman spectra of both samples exhibited typical G and 2D bands at 1580 cm^{-1} and 2680 cm^{-1}, respectively.[31] In general, the G band refers to the stretching regions of C–C bonds, while the 2D band indicates a signature of graphitic sp^2 structures.[32] Besides, D band at 1350 cm^{-1}, which usually refers to the defects, was also observed. These defects can be obtained from vacancies of the atom, grain boundaries, and doping atoms in graphene, or amorphous parts.[33] Also, the G + D band, appeared at 2910 cm^{-1}, generally relates to the presence of the highly disordered carbon.[34] Moreover, I_D/I_G ratio was also calculated from the intensities of D band and G band. I_D/I_G ratio is normally used to indicate the degree of graphitization, which is one of the key factors to determine the perfection of the carbon plane.[35] The I_D/I_G ratio of Cu-NFG-100 (0.77) was found to be higher than that of Cu-NFG-200 (0.72). As the shred of evidence, Cu-NFG-100 had more defect sites on the carbon framework than Cu-NFG-200. In addition, the degree of disorder on carbon materials could be further confirmed by the disorder parameters of $I_D/(I_D + I_G)$ ratio and width of D-band, W_D. The higher values are the higher degree of disorder. Our samples showed the values of $I_D/(I_D + I_G)$ at 0.436 and 0.420 and of W_D at 90.01 and 87.62 cm^{-1} for Cu-NFG-100 and Cu-NFG-200, respectively. These values referred low degree of disorder of graphitic plane and they were in good agreement as in previous reported.[36] The same result was previously reported that the higher repetition frequency led to a larger amount of energy, which could cause similar phenomenon as carbonization, resulted in the carbon with the ordered structure and low defects.[37] Additionally, full width at half maximum of the 2D band ($FWHM_{2D}$) and the intensity ratio of 2D and G bands were also calculated. The I_{2D}/I_G ratios of Cu-NFG-100 and Cu-NFG-200 were 0.57 and 0.61, respectively. The $FWHM_{2D}$ value of Cu-NFG-100 was 89.5 cm^{-1}, while that of Cu-NFG-200 was 71.4 cm^{-1}. The obtained values of I_{2D}/I_G and $FWHM_{2D}$ could confirm that the encapsulating shell was few-layer graphene.[38,39] The I_{2D}/I_G ratio and $FWHM_{2D}$ of Cu-NFG-100 implied that the number of layers in the encapsulating shell was higher than that of Cu-NFG-200.[39] Therefore, the XRD and Raman results could suggest that Cu nanoparticles encapsulated by few-layer graphene could be prepared by the SP process.

The surface chemical compositions and elemental bonding states of the obtained samples were demonstrated by XPS analysis. According to Table 1, both samples, Cu-NFG-100 and Cu-NFG-200 showed the nitrogen and oxygen contents, which could be generated by the decomposition and recombination of DMF molecules during the SP process. Besides, the atomic composition of Cu in Cu-NFG-100 illustrated lower than that of Cu-NFG-200, which was consistent with the TGA result (Fig. S2†). To understand the atomic-level details, the deconvolution was applied to the high-resolution XPS spectra to explore the chemical states of each element shown in Fig. 4. At a high resolution, the C 1s spectra were deconvoluted into five peaks and shown in Fig. 4a and d. The strong peak at 284.3 ± 0.1 eV represented C–C for the carbon sp^2 structures of NFG. In addition, the presence of C–N, C–O, C═O, and O–C═O bonding peaks at 285.4 ± 0.2 eV, 285.8 ± 0.1 eV, 286.6 ± 0.2 eV, and 289.2 ± 0.2 eV, respectively, was also observed, implying that the graphene planes were functionalized by nitrogen and oxygen.[40] The bonding states of N atoms were analyzed by deconvolution into four subspecies, including pyridinic N at 398.6 ± 0.2 eV, pyrrolic N at 399.5 ± 0.2 eV, quaternary N peak at 401.3 ± 0.2 eV and oxidized N at 403.2 ± 0.2 eV (Fig. 4b and e). The pyridinic N, pyrrolic N, and oxidized N usually refer to the nitrogen functional groups at the edge of carbon frameworks, while the quaternary N is a substituent in the framework.[41] Both Cu-NFG-100 and Cu-NFG-200 had pyrrolic N and pyridinic N as the major species, as well as, the quaternary N which could confirm the doping of nitrogen atoms into the carbon framework *via* the SP process. Different ratios of nitrogen doping types provided various catalytic performance for reactions.[42] According to Fig. 4c and f, the high-resolution Cu $2p_{3/2}$ spectra were deconvoluted into two states including Cu(0) at 932.7 ± 0.1 eV and Cu(II) at 934.6 ± 0.1 eV.[43] The ratios of Cu(II)/Cu(0) were 0.088 and 0.174 in Cu-NFG-100 and Cu-NFG-200, respectively, indicating that Cu-NFG-200 contained more oxidized Cu-core which was in good agreement with the XRD results. Furthermore, electrical resistivity was also measured by the 2-probe method. The resistivities of Cu-NFG-100 and Cu-NFG-200 were found to be 1.72 Ω cm and 1.37 Ω cm, respectively. The slightly higher value of resistivity on Cu-NFG-100 than Cu-NFG-200 might be caused by a thicker layer of the shell. According to the previous study, the shell thickness of the core–shell nanostructure was found to be inversely proportional to the resistivity, because electrons can flow through an in-plane structure, but not between planes.[44]

Table 1 The surface elemental composition obtained from XPS for Cu-NFG-100 and Cu-NFG-200

Sample	C (at%)	N (at%)	O (at%)	Cu (at%)	N/C	O/C	Cu/C
Cu-NFG-100	90.94	3.93	4.53	0.60	0.04	0.05	0.01
Cu-NFG-200	90.24	3.73	3.36	2.68	0.04	0.04	0.03

3.2 Proposed synthesis mechanism of Cu-NFGs using solution plasma

The possible mechanism for the formation of core–shell nanostructure by the SP process at different repetition frequencies was also proposed in this study, aiming to give deep understanding the simultaneous synthesis of metal nanoparticles as core and few-layer graphene as a shell. According to the gathered evidence in this study, the core–shell nanostructure, *i.e.*, Cu nanoparticle encapsulated by NFG, could be generated by the combination of two major reactions. One was the carbonization to form carbon materials as shell and another one was the plasma sputtering at the tip of metal electrodes to generate metal atoms which lead to the formation of the metal–core. In the SP process, the DMF molecules were decomposed in the plasma zone, where the temperature were found to be 3500

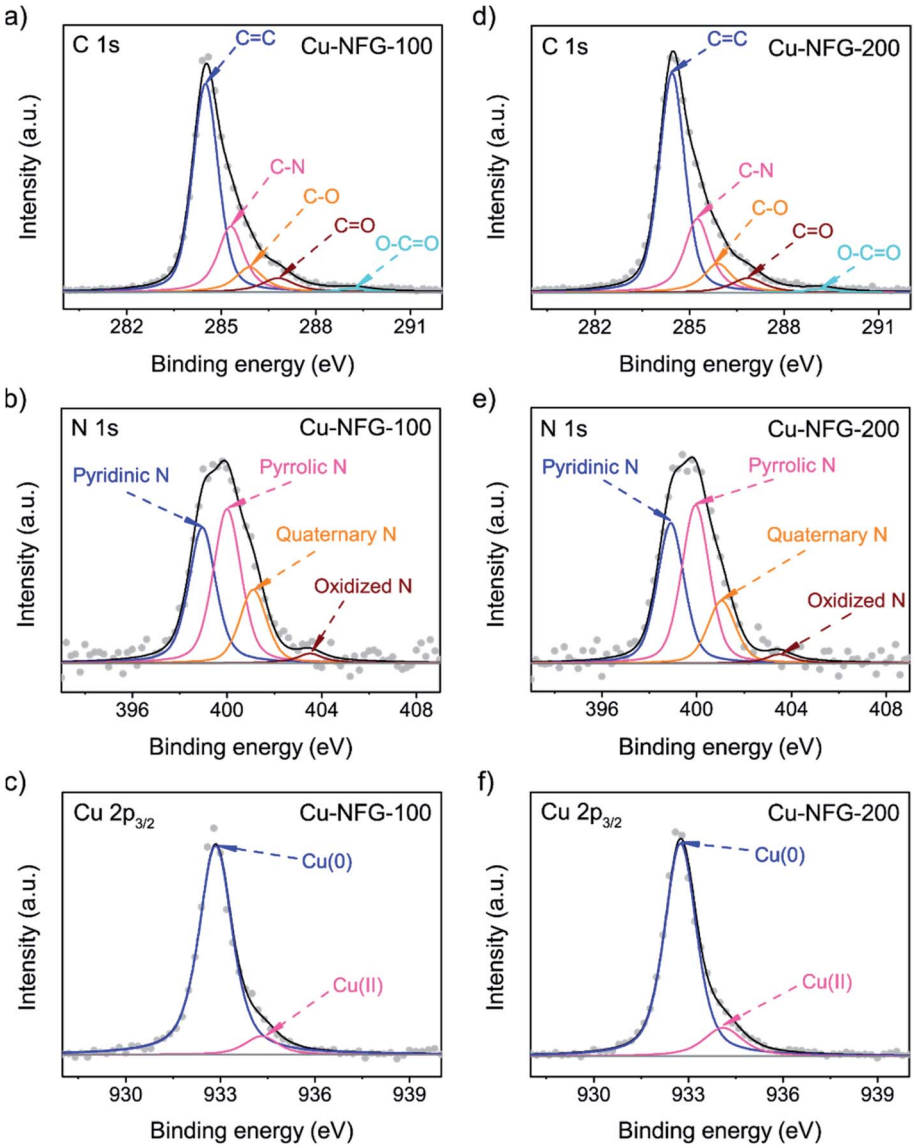

Fig. 4 XPS at high-resolution spectra of C 1s (a and d), N 1s (b and e), and Cu $2p_{3/2}$ (c and f) of Cu-NFG-100 and Cu-NFG-200.

K and 3660 K at 100 kHz and 200 kHz of repetition frequencies, respectively. The bonds between carbon atoms in DMF were broken down to form radicals and fragments. Later, those fragments were propagated and recombined to form a carbon framework. However, the formation and extension of carbon structure were quenched as diffusing to the surrounding solution-phase where the temperature was extremely low (*i.e.*, room temperature), compared to that of the plasma zone. In the previous studies, it was found that the carbon formation in aromatic compounds, such as benzene, was rapidly occurred due to the presence of delocalization of π electrons.[45–48] The generated radicals from the decomposition of organic molecules could propagate with the neighboring molecules to perform polymerization, obtaining an extensive framework.[12] However, in this case, the carbon precursor was DMF which is an aliphatic compound without a delocalization system. Therefore, the rate of carbon formation was relatively low, compared to that of aromatic compounds. Besides, nitrogen and oxygen atoms, presented in the DMF molecules, could cause the terminating sites which limited the further growth of the carbon structure.[22] For the formation of Cu nanoparticles as the core of Cu-NFG, the Cu nanoparticles could be synthesized by the plasma sputtering at the tips of electrodes without using any other chemicals, like reducing agents. The metal atoms at electrodes were struck, bombarded, and knocked off by the energized atoms, ions, and electrons in the plasma gas phase during the plasma discharge.[49] The ejected metal atoms could lead to the nucleation, followed by crystal growth to a larger cluster and nanoparticle. Simultaneously, the crystal growth of metal also cooperated with graphene formation. The surface of metal acts as a substrate for the adsorption of pre-formed single layer carbon.[50] In the beginning, the NFG layers should show an amorphous phase, due to the stochastic collisions of radicals.[51] However, there was an extremely high temperature in the

plasma zone and plasma interfaces, which can graphitize those carbons to become an ordered crystalline layer or graphene,[52] resulting in carbon–Cu composite nanoaggregates. Then, those aggregates agglomerated and coalesced each other to form a single Cu–core, which was favorable under high temperature in the plasma zone. While there was an instantaneous inter-diffusion of carbon out of the composites due to the low solubility limit of carbon in Cu at high temperature at the plasma zone giving a Cu–core with very low or no defects.[53] This was corresponding to our TEM results (Fig. 2) where the crystal plane of Cu can be seen clearly and uniformly. The carbon growth to form multiple layers of NFG might result in an amorphous phase at first, due to the stochastic collisions of radicals. However, there was an extremely high temperature in the plasma zone as well as plasma interfaces that can graphitize those carbons to become an ordered crystalline layer.[52] After that, when the synthesized product diffused through the interface zone to a bulk liquid which has much lower temperature leading the reactions to be suddenly quenched. According to the quenching process, the thermodynamically metastable products could be formed under this condition in which the conventional method is unable to achieve that.[15] Fig. 5 illustrates the core–shell structure synthesis pathway by the SP process. Moreover, as a result of this study, it was found that adjusting repetition frequencies could help to control the thickness of the carbon–shell on the metal–core. The waveforms of SP process at 100 kHz and 200 kHz are shown in Fig. S4.† The energy per pulse (E_p) can be calculated by integration of power (voltage times ampere) at any instant of time, whereas the energy per time (E_t) is a product of energy per pulse multiplying with the pulse frequency$E_p = \int (V_t \times I_t) dt$ and $E_t = f \times E_p$ where $V_t$and I_t are applied voltage and ampere at any t, whereas f is a repetition frequency of discharge. When the frequency is doubled, the number of striking is also doubled, but the energy strike per pulse is the same since the current and voltage detected is still the same. This refers to no change in the amount of energy per pulse but increasing in the amount of energy per time. The increment of the number of striking leads to a faster rate of the synthesis. The number of striking to the metal electrode at 200 kHz is greater resulting in more metal atoms ejecting from the electrodes causing metal nanoparticles size bigger. This was in good agreement to the mean particles size in our TEM results (Fig. 2), that it shifted to a bigger size when applying higher frequency, as well as a higher production rate was obtained at a higher frequency of 200 kHz. In addition, the number of NFG layers coating on Cu–core was found in TEM results. There were about three to five layers of NFG on Cu-NFG-100, whereas Cu-NFG-200 was found to be one to three layers. As mentioned above, increasing the frequency does not increase the energy per pulse but the energy in a period. Therefore, the chemical composition of radicals formed were the same. As can be seen in Fig. 1b, the radicals' formations were similar referring the type of bond broken supposed to be similar as well. From our XPS results (Table 1) showed that the composition of carbon–shell of both Cu-NFGs were indistinguishable. Although, the number of striking by plasma gas was more frequent at 200 kHz leading to a faster rate of carbon formation. However, it seemed the rate of metal sputtering was enhanced with greater influence than the increase of the rate of carbon formation at higher frequency. This resulted the shell thickness, as well as the number of NFG layers coating on Cu-NFG-200 was lower than of Cu-NFG-100. Therefore, the number of shells on Cu-NFG was negatively influenced by increasing repetition frequency. In this study, it was unlike the synthesis of metal decorated on carbon support as reported in previous studies.[45–48] Those used aromatic compounds to generate nanocarbons extremely faster relative to metal sputtering rate, resulting in a low amount of metal on a carbon nanosphere supports.

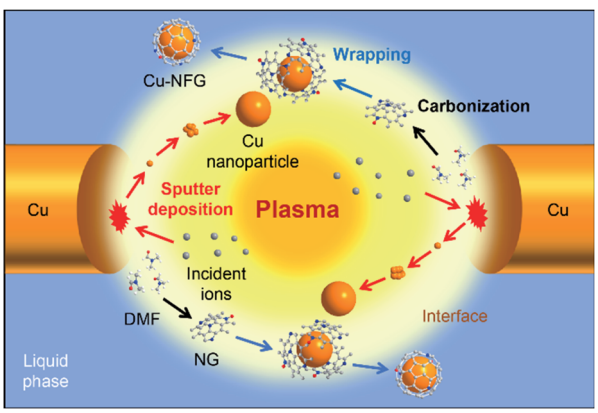

Fig. 5 Illustration core–shell structure synthesis of Cu-NFG *via* solution plasma.

3.3 Chemical resistance ability in acidic solution

The chemical stability of the synthesized product was also investigated by using acid immersion tests, using separated HNO_3 and H_2SO_4, in order to study the protective ability of the NFG-shell. Generally, Cu atoms would react with nitrate ions *via* redox reaction, since the E^0 of NO_3^-/NO (E^0 = +0.96 V (V *vs.* SHE)) is more favorable than of Cu^{2+}/Cu (E^0 = +0.34 V (V *vs.* SHE)). Therefore, Cu could get oxidized to form Cu^{2+} by nitrate ions in an acid medium. Therefore, the measurements were first done using a strong acid of 1 N HNO_3 at 25 °C. The amount of the dissolved Cu ions from the samples immersed in the testing solutions were determined by ICP-OES (Fig. 6a). After 1 h of immersion, commercial bare Cu showed the concentration of Cu ions about 59.2 ppm. Further increasing immersion time to 2 and 4 hours, respectively, did not change the concentration significantly. This means all commercial Cu had been completely dissolved implying that there was no protectability for this bare Cu. Meanwhile, the Cu particles from the Cu electrode gave the concentration of Cu ions at 64.8 ppm after 48 h of the immersion. For Cu-NFG-200 immersed in the testing solution after 1 h, the concentration of Cu ions was 3.4 ppm and gradually increased to the highest value of 6.9 ppm after immersion for 48 h. The Cu-NFG-100 exhibited the highest concentration of Cu ions at 2.8 ppm after immersion for 48 h, which could be considered as the best protectability, compared

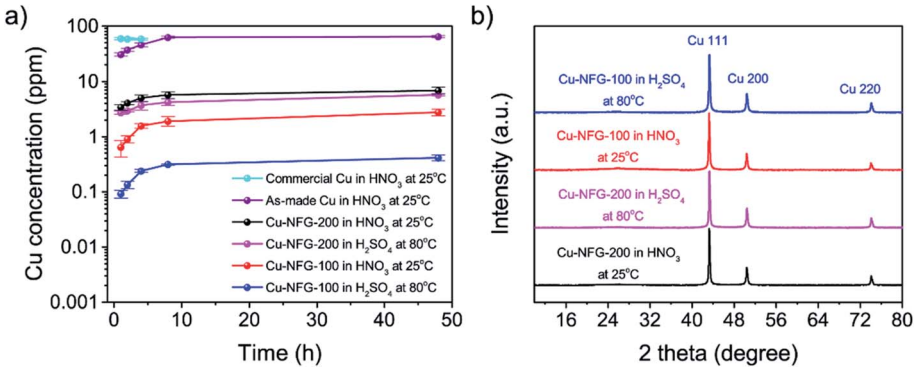

Fig. 6 ICP-OES of Cu ion concentration in the collected solution (a) and XRD of solid residues (b) results of the tested samples from the immersion tests in acid.

to other samples. Accordingly, it could be suggested that the NFG-shell played a very important role in protecting the metal core and the thickness of NFG-shell or the number of layers could be a key factor for promoting or maintaining the stability of core–shell materials or catalysts. Typically, the corrosion rate depends on a surface area of a material. To make a fair comparison, the corrosion rates per surface area of the sample in cm^2 were calculated. The surface area of Cu-NFG-100 and Cu-NFG-200 (Fig. S5†) were found to be similar at 71.73 and 75.36 $m^2\ g^{-1}$, respectively. The results are summarized in Table 2. In the beginning, Cu-NFG-200 showed a relatively high corrosion rate, compared to that of Cu-NFG-100, which could be caused by the incompletely covered shell on Cu–core. The rates of corrosion of Cu-NFG-200 were about 2 to 5 times higher in nitric acid immersion and about 13 to 28 times higher in sulfuric acid immersion compared to Cu-NFG-100. These differences can be explained by the effectiveness of the protective coating layer. In the case of Cu-NFG-100, it had a thicker layer of coating at 3 to 5 layers which provided better protection, whereas Cu-NFG-200 had 1 to 3 layers of coating and imperfect coating as shown in TEM results in Fig. 2. This also is in good agreement of the XRD pattern (Fig. 3a) that confirmed the imperfect coating that the peak of CuO can be observed on Cu-NFG-200. Surprisingly, Cu-NFG-100 could withstand the immersion at a higher temperature. There was just only 0.4 ppm of Cu ions were showed in the ICP-OES measurement, as well as the lowest corrosion rate was obtained. Moreover, the XRD measurement was also used to observe the structural change of the products after the immersion test, as shown in Fig. 6b. It was clearly observed that the XRD pattern of Cu-NFG-200 changed, while Cu-NFG-100 could excellently maintain its structure after tested with HNO_3 and H_2SO_4. Therefore, the NFG-shell could satisfy to protect Cu–core, which was synthesized by the SP process using the repetition frequency at 100 kHz, from acid–corrosion and oxidation even in high operating temperature.

Table 2 Calculated corrosion rates of Cu-NFG-100 and Cu-NFG-200 in 1 N HNO_3 at 25 °C and Cu-NFG-100 in 1 N H_2SO_4 at 80 °C

Corrosion time (h)	Corrosion rate in HNO_3 ($\times 10^{-12}$ mol cm^{-2} h^{-1})		Corrosion rate in H_2SO_4 ($\times 10^{-12}$ mol cm^{-2} h^{-1})	
	$W_{Cu\text{-}NFG\text{-}100}$	$W_{Cu\text{-}NFG\text{-}200}$	$W_{Cu\text{-}NFG\text{-}100}$	$W_{Cu\text{-}NFG\text{-}200}$
1	2.308	11.721	0.334	9.377
2	1.642	6.982	0.244	5.051
4	1.418	4.328	0.217	3.175
8	0.867	2.461	0.141	1.822
48	0.208	0.495	0.031	0.414

4. Conclusion

Cu nanoparticles encapsulated with N-doped few-layer graphene was successfully synthesized in one pot *via* SP using only DMF as the reaction solution under room temperature and pressure condition. The number of N-doped few-layer graphene layers could be tuned by adjusting a repetition frequency to achieve the appropriate number of layers, which could result in the outstanding stability of the obtained product in acid mediums. Moreover, not only the structure but also functionalization, such as doping of N atoms onto graphene structure, can be adjusted, depending on the type of precursors and electrodes. This leads to the performance improvement of the obtained materials to suit desired applications, for instance, to be a durable electrocatalyst for metal–air electrochemical cell, thermally conductive adhesives, and a conductive printing. Accordingly, SP showed ability as a promising tool that can explore a new opportunity, aiming to achieve a tunable synthesis of not the only core–shell structure but also other advanced materials, that can meet economic feasibility and environmental concerns.

Conflicts of interest

There are no conflicts to declare.

Acknowledgements

This work has been financially supported by Japan Science and Technology Corporation-Strategic International Collaborative Research Program (Grant number: JPMJSC18H1) and Japan Science and Technology Corporation-Open Innovation Platform with Enterprises, Research Institute and Academia (Grant

number: JPMJOP1843). The author also acknowledges the study support from JICA Technical Cooperation Project for ASEAN University Network/Southeast Asia Engineering Education Development Network (Program number: J-1710176).

References

1 S. K. Tiwari, S. Sahoo, N. Wang and A. Huczko, *Journal of Science: Advanced Materials and Devices*, 2020, **5**, 10–29.
2 D. Selvakumar, H. Sivaram, A. Alsalme, A. Alghamdi and R. Jayavel, *J. Mater. Sci.: Mater. Electron.*, 2016, **27**, 6232–6241.
3 S. Wang, X. Huang, Y. He, H. Huang, Y. Wu, L. Hou, X. Liu, T. Yang, J. Zou and B. Huang, *Carbon*, 2012, **50**, 2119–2125.
4 M. Topsakal, H. Şahin and S. Ciraci, *Phys. Rev. B: Condens. Matter Mater. Phys.*, 2012, **85**, 155445.
5 G. Panomsuwan, N. Saito and T. Ishizaki, *Phys. Chem. Chem. Phys.*, 2015, **17**, 6227–6232.
6 S. Chen, A. Zehri, Q. Wang, G. Yuan, X. Liu, N. Wang and J. Liu, *ChemistryOpen*, 2019, **8**, 58–63.
7 W. Lei, H. M. Barnes, J. Zhang and Z. Cai, *Wood Fiber Sci.*, 2017, **49**, 22–32.
8 J. Li and C.-y. Liu, *New J. Chem.*, 2009, **33**, 1474–1477.
9 H.-m. Kim, N. Saito and D.-w. Kim, *ChemistrySelect*, 2018, **3**, 6302–6308.
10 E. Antolini, *Energy Environ. Sci.*, 2009, **2**, 915–931.
11 C. Mattevi, H. Kim and M. Chhowalla, *J. Mater. Chem.*, 2011, **21**, 3324–3334.
12 T. Morishita, T. Ueno, G. Panomsuwan, J. Hieda, A. Yoshida, M. A. Bratescu and N. Saito, *Sci. Rep.*, 2016, **6**, 36880.
13 X. Hu, X. Shen, O. Takai and N. Saito, *J. Alloys Compd.*, 2013, **552**, 351–355.
14 N. Saito, M. A. Bratescu and K. Hashimi, *Jpn. J. Appl. Phys.*, 2017, **57**, 0102A0104.
15 H. Yui and M. Banno, *Jpn. J. Appl. Phys.*, 2017, **57**, 0102A0101.
16 S. Chae, G. Panomsuwan, M. A. Bratescu, K. Teshima and N. Saito, *ACS Appl. Nano Mater.*, 2019, **2**, 1350–1355.
17 M. A. Bratescu, O. Takai and N. Saito, *J. Alloys Compd.*, 2013, **562**, 74–83.
18 G. Panomsuwan, S. Chiba, Y. Kaneko, N. Saito and T. Ishizaki, *J. Mater. Chem. A*, 2014, **2**, 18677–18686.
19 D.-w. Kim, O. L. Li and N. Saito, *Phys. Chem. Chem. Phys.*, 2015, **17**, 407–413.
20 C. Chokradjaroen, S. Kato, K. Fujiwara, H. Watanabe, T. Ishii and T. Ishizaki, *Sustainable Energy Fuels*, 2020, 4570–4580.
21 O. L. Li, S. Chiba, Y. Wada, G. Panomsuwan and T. Ishizaki, *J. Mater. Chem. A*, 2017, **5**, 2073–2082.
22 K. Kim, K. Hashimi, M. A. Bratescu and N. Saito, *Nanosci. Nanotechnol. Lett.*, 2018, **10**, 814–819.
23 F. Rezaei, Y. Gorbanev, M. Chys, A. Nikiforov, S. W. Van Hulle, P. Cos, A. Bogaerts and N. De Geyter, *Plasma Processes Polym.*, 2018, **15**, 1700226.
24 P. Pootawang, N. Saito and S. Y. Lee, *Nanotechnology*, 2013, **24**, 055604.
25 Z. Zhang, Y. Ji, J. Li, Z. Zhong and F. Su, *RSC Adv.*, 2015, **5**, 54364–54371.
26 H. Wu, T. Peng, Z. Kou, J. Zhang, K. Cheng, D. He, M. Pan and S. Mu, *Chin. J. Catal.*, 2015, **36**, 490–495.
27 D. M. McClenathan, W. C. Wetzel, S. E. Lorge and G. M. Hieftje, *J. Anal. At. Spectrom.*, 2006, **21**, 160–167.
28 L. Hang, Y. Zhao, H. Zhang, G. Liu, W. Cai, Y. Li and L. Qu, *Acta Mater.*, 2016, **105**, 59–67.
29 S. Pourbeyram, J. Abdollahpour and M. Soltanpour, *Mater. Sci. Eng., C*, 2019, **94**, 850–857.
30 Z.-L. Cheng and X.-X. Qin, *Chin. Chem. Lett.*, 2014, **25**, 1305–1307.
31 J.-B. Wu, M.-L. Lin, X. Cong, H.-N. Liu and P.-H. Tan, *Chem. Soc. Rev.*, 2018, **47**, 1822–1873.
32 S. Samanta, S. Singh and R. R. Sahoo, *RSC Adv.*, 2015, **5**, 61888–61899.
33 A. Yadegari, L. Samiee, S. Tasharrofi, S. Tajik, A. Rashidi, F. Shoghi, M. Rasoulianboroujeni, M. Tahriri, S. J. Rowley-Neale and C. E. Banks, *RSC Adv.*, 2017, **7**, 55555–55566.
34 L. Bokobza, J.-L. Bruneel and M. Couzi, *C*, 2015, **1**, 77–94.
35 M. Mowry, D. Palaniuk, C. C. Luhrs and S. Osswald, *RSC Adv.*, 2013, **3**, 21763–21775.
36 A. Cuesta, P. Dhamelincourt, J. Laureyns, A. Martinez-Alonso and J. D. Tascón, *Carbon*, 1994, **32**, 1523–1532.
37 K. Hyun, T. Ueno and N. Saito, *Jpn. J. Appl. Phys.*, 2015, **55**, 01AE18.
38 J.-S. Hwang, Y.-H. Lin, J.-Y. Hwang, R. Chang, S. Chattopadhyay, C.-J. Chen, P. Chen, H.-P. Chiang, T.-R. Tsai and L.-C. Chen, *Nanotechnology*, 2012, **24**, 015702.
39 A. C. Ferrari, J. Meyer, V. Scardaci, C. Casiraghi, M. Lazzeri, F. Mauri, S. Piscanec, D. Jiang, K. Novoselov and S. Roth, *Phys. Rev. Lett.*, 2006, **97**, 187401.
40 N. Thongwichit, O. L. H. Li, W. Yaowarat, N. Saito and U. Suriyapraphadilok, *Jpn. J. Appl. Phys.*, 2015, **55**, 01AE10.
41 D.-w. Kim, O. L. Li and N. Saito, *Phys. Chem. Chem. Phys.*, 2014, **16**, 14905–14911.
42 D. Guo, R. Shibuya, C. Akiba, S. Saji, T. Kondo and J. Nakamura, *Science*, 2016, **351**, 361–365.
43 F. Liu, L. Csetenyi and G. M. Gadd, *Appl. Microbiol. Biotechnol.*, 2019, **103**, 7217–7230.
44 X.-Y. Fang, X.-X. Yu, H.-M. Zheng, H.-B. Jin, L. Wang and M.-S. Cao, *Phys. Lett. A*, 2015, **379**, 2245–2251.
45 J. Kang, Y. Kim, H. M. Kim, X. Hu, N. Saito, J. H. Choi and M. H. Lee, *Sci. Rep.*, 2016, **6**, 38652.
46 J. Kang, O. L. Li and N. Saito, *Nanoscale*, 2013, **5**, 6874–6882.
47 J. Kang and N. Saito, *RSC Adv.*, 2015, **5**, 29131–29134.
48 D.-w. Kim, O. L. Li, P. Pootawang and N. Saito, *RSC Adv.*, 2014, **4**, 16813–16819.
49 F. Yu, M. Liu, C. Ma, L. Di, B. Dai and L. Zhang, *Nanomaterials*, 2019, **9**, 1436.
50 Y. Dedkov and E. Voloshina, *J. Phys.: Condens. Matter*, 2015, **27**, 303002.
51 C. O. Reinhold, P. S. Krstic and S. Stuart, *Nucl. Instrum. Methods Phys. Res., Sect. B*, 2009, **267**, 691–694.
52 M. A. Pimenta, G. Dresselhaus, M. S. Dresselhaus, L. G. Cancado, A. Jorio and R. Saito, *Phys. Chem. Chem. Phys.*, 2007, **9**, 1276–1291.
53 G. A. López and E. J. Mittemeijer, *Scr. Mater.*, 2004, **51**, 1–5.